

# The Faint Sky Variability Survey II: Initial Results

M. E. Everett<sup>1</sup>, S. B. Howell<sup>1</sup>, M. E. Huber<sup>1</sup>,  
 P. J. Groot<sup>2</sup>, P. M. Vreeswijk<sup>3</sup>, J. van Paradijs<sup>3,4</sup>,  
 D. Davis<sup>5</sup>, C. Neese<sup>5</sup>, H. Scholl<sup>6</sup>,  
 E. P. J. van den Heuvel<sup>3</sup>, T. Augusteijn<sup>7</sup>, H. Böhnhardt<sup>8</sup>,  
 P. A. Charles<sup>9</sup>, T. J. Galama<sup>10</sup>, E. Kuulkers<sup>11,12</sup>,  
 C. Kouveliotou<sup>13</sup>, C. Moreno<sup>14</sup>, G. Nelemans<sup>3</sup>,  
 R. Rebolo<sup>15</sup>, R. G. M. Rutten<sup>7</sup>, J. Storm<sup>16</sup>,  
 N. Tanvir<sup>17</sup>, L. B. F. M. Waters<sup>3</sup>, R. A. M. J. Wijers<sup>18</sup>

<sup>1</sup>*Astrophysics Group, Planetary Science Institute, 620 N. 6th Ave., Tucson, AZ, USA*

<sup>2</sup>*Harvard-Smithsonian Center for Astrophysics, 60 Garden St., Cambridge, MA 02138, USA*

<sup>3</sup>*Astronomical Institute ‘Anton Pannekoek’/ CHEAF, Kruislaan 403, 1098 SJ, Amsterdam, the Netherlands*

<sup>4</sup>*Physics Department, University of Alabama in Huntsville, Huntsville, AL, USA*

<sup>5</sup>*Planetary Science Institute, 620 N. 6th Ave., Tucson, AZ, USA*

<sup>6</sup>*Observatoire de la Côte d’Azur, Nice, France*

<sup>7</sup>*Isaac Newton Group of Telescopes, Apartado de Correos 321, Santa Cruz de La Palma, La Palma, Spain*

<sup>8</sup>*European Southern Observatory, Casilla 19001, Santiago 19, Chile*

<sup>9</sup>*Astronomy Department, University of Southampton, Southampton, UK*

<sup>10</sup>*Astronomy Department, California Institute of Technology, Pasadena, CA, USA*

<sup>11</sup>*Space Research Organization Netherlands, Sorbonnelaan 2, 3584 CA, Utrecht, the Netherlands*

<sup>12</sup>*Astronomical Institute, Utrecht University, P.O. Box 80000, 3507 TA Utrecht, The Netherlands*

<sup>13</sup>*Marshall Space Flight Center (NASA), Huntsville, AL, USA*

<sup>14</sup>*Nordic Optical Telescope, La Palma, Spain*

<sup>15</sup>*Instituto de Astrofísica de Canarias, La Laguna, Tenerife, Spain*

<sup>16</sup>*Astrophysikalische Institut Potsdam, An der Sternwarte 16, 14482 Potsdam, Germany*

<sup>17</sup>*Astronomy Department, University of Hertfordshire, Hertfordshire, UK*

<sup>18</sup>*Department of Physics and Astronomy, SUNY, Stony Brook, NY 11794-3800, USA*

## ABSTRACT

We discuss the first results from the Faint Sky Variability Survey (Groot et al. 2000). The data consist of  $V$ -band light curves,  $BVI$  colours, astrometry, and morphology information on several hundred thousand point and extended sources in the magnitude range  $V = 17 - 25$ . We discuss the first 30 survey fields covering an area of 8.4 square degrees towards moderate and high galactic latitudes. We analyse the quality of and discuss our differential photometry light curves. We employ statistical methods to select variable objects and present example variable light curves. The distribution of the colours and magnitudes of point sources in the survey is discussed and compared to galactic star count models. Finally, we discuss our search for trans-Neptunian objects in the FSVS fields observed towards ecliptic opposition.

**Key words:** surveys – stars: statistics – stars: variables: other

## 1 INTRODUCTION

The Faint Sky Variability Survey (hereafter FSVS) has been discussed by Groot et al. (2000; hereafter paper I) and is part of the Wide Field Survey. The primary goals of the FSVS is to quantify the photometric and astrometric variability

of faint sources at moderate to high galactic latitudes and to identify objects for detailed follow-up observations. The first two FSVS observing runs cover 8.4 square degrees to a  $5\text{-}\sigma$  limiting magnitude  $V \sim 25$  for point sources, providing  $V$ -band light curves,  $BVI$  colours, and morphological and astrometric information for all objects in the field.

The dataset of the FSVS allows us to detect rare stellar and galactic populations exhibiting photometric variability, objects with high proper motions or extreme colours, and trans-Neptunian objects. In this paper we present initial results from the FSVS. In Section 2 we review the observations that are discussed in paper I, in Section 3 we discuss the differential photometric techniques used in the FSVS, and in Section 4 we show results.

## 2 OBSERVATIONS

We took the first observations for the FSVS on 1998 Nov. 16-21 UT, and a second observing run was taken on 1999 May 11-17 UT. The observing strategy has been detailed in paper I so we describe it only briefly here. Each pointing of the telescope is centered on a different “field”, consisting of the area imaged by the four Wide Field Camera CCDs (each of the 4100x2048 pixel CCDs images an area of 0.072 sq. degrees for a total of 0.29 sq. degrees per field with a plate scale of  $0''.33 \text{ pixel}^{-1}$ ). The total area of the sky covered during these first two runs is 8.4 square degrees. Each field is observed 10-20 times with 10 minute exposures in the *V*-band providing time sampling from  $\sim 13$  minutes up to, typically, 5 days. Additionally, each field is observed once with exposures of 10 and 15 minutes respectively in the *B*- and *I*-bands to provide colour information. Astrometric plate solutions are found by taking positions from the USNO-A2.0 Catalog (Monet et al. 1996). Magnitudes are put on a standard scale using observations of Landolt standard star fields taken in succession with our data fields on the night that we observe the field in *BVI*.

The 18 fields observed during the November run clustered in three “areas” of the sky, and the 12 observed during the May run were clustered in two additional areas. In this way, the FSVS samples a variety of different galactic and ecliptic environments, each chosen to avoid regions of obvious interstellar extinction so that distant parts of the galactic halo could be observed. Approximately one year after each field is first observed it is scheduled for re-observation with a single 10-minute *V*-band exposure to identify high proper motion objects and those exhibiting long-term photometric variability. The areas observed during the first two FSVS observing runs are listed in Table 1.

## 3 DIFFERENTIAL PHOTOMETRY

The light curves produced for every object in the FSVS are the result of ensemble differential aperture photometry, wherein the observed flux of each object is corrected for variations in atmospheric transparency and seeing by comparing the observed fluxes to those of a set of bright, non-variable calibration stars simultaneously observed on the same CCD (hereafter referred to as reference stars). The techniques and application of such differential photometry are discussed by Howell, Mitchell, & Warnock (1988), Honeycutt (1992), and Everett & Howell (2000). Because the FSVS dataset contains a large number of sources, includes a wide range of object types (point and extended sources), and was observed with a wide field and under different observing conditions (seeing and transparency), it presents a good test for our methods

of photometry. Note that here we are concerned with the internal precision of each light curve, and this depends only on comparisons between the reference stars and each object. This internal precision is distinct from our calibration of the magnitude scale obtained through observations of separate photometric standard star fields.

Our ability to perform precise differential photometric measurements depends on reducing a combination of random and systematic uncertainties to its lowest possible level. Random errors arise from the finite number of detected photons from the star and sky and readout noise. The magnitude of these random errors can be calculated in a straightforward manner using Poisson statistics. Systematic errors arise mainly from imperfections in the instrumentation and calibration which normally only become noticeable once the random sources of noise are reduced to  $< 1$  percent. Sources of systematic errors in the light curves include guiding errors, scattered light, flatfielding uncertainties, and colour-dependent extinction. It is particularly important to understand the sources and behaviour of these systematic errors because they can produce artifacts in light curves that might otherwise be attributed to real variations.

The two-dimensional profiles of objects in the FSVS differ due to intrinsic differences (galaxies vs. stars), extrinsic differences (e.g., crowding), as well as instrumental or observational effects (e.g., optical aberrations, seeing changes, guiding errors). For differential photometry we use the SExtractor package (Bertin & Arnouts 1996) with circular apertures that allow an exact comparison of the fluxes from two objects having the same profile. This assumes that although the entire flux from each object is not contained within the aperture, the same fraction of the flux will be. This assumption breaks down if one attempts to compare the fluxes from two objects with different profiles. For instance, these effects prevent us from obtaining the high photometric precision light curves for galaxies (which have unique profiles) that we have for stars. Stars too may have asymmetric profiles due to guiding errors or they may be overlapped by the profiles of neighbouring objects. In these cases we either reject the data or interpret it with caution.

The systematic errors produced by differences and asymmetries in the profiles of the reference stars and objects in the field may manifest themselves as artificial “variations” in the objects’ light curves. Fortunately, we can distinguish these artifacts from true variations because they are inter-correlated and often depend on variations in the seeing (light curves of crowded or extended objects tend to exhibit the same artificial patterns). The following measures are taken to reduce these artifacts and to reject problematic objects from the dataset:

1. We reject the very few images taken with poor guiding.
2. We measure magnitudes using four different circular aperture sizes centered on each object. The largest aperture is optimal for the brightest stars (for which photometric precision is highest). The larger apertures reduce the adverse effects of slight differences between the profiles of the reference stars and those of objects of interest. This is because a smaller fraction of the total flux falls outside of large apertures, meaning any differences in the profile are less important. Other sources of uncertainty such as sky noise dom-

**Table 1.** Areas observed in the FSVS up to May 1999

Fields	$\alpha_{2000}$	$\delta_{2000}$	$l$	$b$
1-6	23 <sup>h</sup> 44 <sup>m</sup>	+27° 2	105°	-33°
7-12	2 <sup>h</sup> 29 <sup>m</sup>	+14° 7	155°	-42°
13-18	7 <sup>h</sup> 54 <sup>m</sup>	+20° 7	200°	+23°
19-24	12 <sup>h</sup> 53 <sup>m</sup>	+27° 0	0°	+90°
27-30	16 <sup>h</sup> 25 <sup>m</sup>	+26° 5	45°	+43°
31,32	17 <sup>h</sup> 20 <sup>m</sup>	+26° 3	49°	+31°

inate for fainter stars. In this case, smaller apertures yield better results.

3. We adopt a high threshold on the “stellarity” parameter to distinguish point sources from extended sources (see paper I for more discussion of the stellarity parameter). This helps us to recognize sources that are close to, but not quite, point-like (e.g., unresolved binaries, compact galaxies). Only light curves of uncrowded point sources can be measured to high precision and realistically searched for variability with errors calculated by Poisson statistics.

4. We choose the reference stars carefully by the method described in paper I. Since the noise in the (non-variable) reference star light curves are uncorrelated, the variance of their mean light curve is easily calculated and is significantly smaller than that of any single object’s light curve. This ensures that no significant noise is added to our light curves based on an uncertain reference star correction.

## 4 RESULTS

After performing the basic data reductions as described in paper I, we are in the position to analyse the data tables. For each source, we have a  $V$ -band light curve, information about the source profile in each exposure (the stellarity parameter and a Gaussian fit to the profile), and  $B$ - and  $I$ -band magnitudes. In addition, coordinates are found for each object. In images where an object is not detected by virtue of its faintness, we have taken our determination of the plate limit as a lower limit to its magnitude. Magnitude measurements that could be in error (e.g., those of objects near bad pixels, the edge of the CCD, crowded by neighbouring sources, or saturated) are flagged and rejected before the analysis.

### 4.1 Magnitudes and Colours

A total of 500,000 objects was detected in the 30 fields (8.4 sq. degrees) observed during our first two FSVS runs. The objects can be classified according to their magnitudes, colours, variability, and stellarity. In Fig. 1 we show the magnitude distribution of point sources and extended sources found in two different galactic regions observed in the FSVS. Here the point sources are taken to be those with stellarity  $> 0.8$  and extended sources include those with stellarity  $< 0.2$ . The thresholds for stellarity are somewhat arbitrary, but for the bright sources these values distinguish point-like from extended sources. For fainter objects there is more confusion distinguishing between point and extended sources due to limited signal-to-noise and the diminishing angular size of galaxies with distance. This means that interpreting Fig. 1 at magnitudes fainter than  $V = 22$  is difficult.

The histogram shows the magnitude range over which we are sensitive ( $V \sim 17 - 25$ ), a range between the brightest stars that remain unsaturated in the 10-minute exposures and our faint detection limit. We also see that the distribution of extended sources rises more steeply at faint magnitudes reflecting the tendency of galaxies to outnumber stars around  $V = 21$ .

In panels (a) of Figs. 2 and 3 we show the magnitude distribution of point sources at two different galactic latitudes alongside the predicted distributions based on the Galaxy models of Bahcall & Soneira (1980). The agreement between the observations and model is generally good to as faint as  $V = 22$ . Towards the North Galactic Pole, we observe an overabundance of point sources between  $V = 21$  and  $V = 22.5$  relative to the model predictions. Some of this excess can be attributed to QSOs (Hartwick & Schade 1990), but stars probably contribute as well. Also, in Figs. 2 and 3, the completeness limits of the survey can be seen to be  $V \sim 22$  for our chosen stellarity threshold of  $> 0.8$ . This is apparent because the observed starcounts per magnitude turn over, whereas the model starcounts continue to increase towards fainter magnitudes. The detection limit is quite a bit fainter than this completeness limit ( $V \sim 25$  compared to  $V \sim 22$ ). One reason is the fact that the stellarity is difficult to measure for the faintest objects, and at low signal-to-noise, all stellarity values tend towards 0.5. Objects fainter than  $V \sim 22$  are in fact detected, but most have stellarity values less than 0.8. Our completeness limit for simply detecting objects in these fields is  $V \sim 24$ . We also note that the completeness and detection limits depend on the observing conditions at the time the data were taken. Some fields are observed under better conditions than others and, naturally, exposures taken during the poorest observing conditions limit our completeness. The detections at  $V \sim 25$  are made on the best exposures. In a similar manner, the bright limit to the survey depends on atmospheric transparency and seeing and this differs between fields. Therefore, the shape of the magnitude distribution at the bright end ( $V = 15 - 17$ ) is statistically uncertain. The panels (b) in Figs. 2 and 3 show the Bahcall & Soneira models broken down into two stellar populations, namely a spheroid and disk component. At the North Galactic Pole, the FSVS contains primarily halo stars whereas at mid-galactic latitudes (e.g., the  $b = +23^\circ$   $l = 200^\circ$  fields shown here), the disk stars dominate.

$BVI$  colours are measured from exposures of the same field taken closely-spaced in time. Thus, for large-amplitude variables, the reported colours should indicate an approximate spectral type. We show a plot of  $V - I$  vs.  $B - V$  for point sources with stellarity  $> 0.8$  in Fig. 4. The major grouping of points traces the main sequence, and the majority of these sources are K and M dwarfs. This can be seen

**Figure 1.** Histograms showing the number of objects vs. magnitude in the 30 fields of the FSVS. The solid curve shows point sources (stellarity $>0.8$ ) and the dotted line shows the same for extended sources (stellarity $<0.2$ ). Both curves rise towards a completeness limit at  $V \sim 22$ , with the extended sources (mainly galaxies) dominating in numbers at magnitudes fainter than  $V \sim 21$ . The faintness limit for actually detecting objects is deeper than  $V \sim 22$ ; objects observed at low signal-to-noise levels are difficult to classify by stellarity as the stellarity tends towards 0.5.

by the labels along the top of the plot that show the  $V - I$  colors expected for main sequence stars. The colours for B-K dwarfs are from Cox (2000) and those for (old disk) M dwarfs are from Leggett (1992). Note that giants in the halo would have similar colours but most would exceed the bright limit of the FSVS. In Fig. 5 we show  $V - I$  vs.  $B - V$  for extended sources with stellarity $<0.2$ . Many galaxy colours cluster around  $V - I = 1.5$  and  $B - V = 0.75$ , falling below the stellar main sequence on this plot. Other galaxies have  $BVI$  colours that place them near the main-sequence or giant branch (the giant branch and main-sequence are difficult to separate on this plot). Note that Figs. 4 and 5 include only those sources detected in every passband and thus, many of the objects with extreme colours are not included since they are undetected at either  $B$  or  $I$ . Similarly, many of the faintest objects are not shown in either Fig. 4 or 5 because we chose not to include those with stellarity values between 0.2 and 0.8. Faint objects with such stellarity values are difficult to classify.

We show histograms of the distribution of objects in  $B - V$  in Figs. 6 and 7. We have included only point sources in these plots by requiring stellarity $>0.8$  and  $17 < V < 22$ . The magnitude limits are chosen because the FSVS is complete within these limits for the point sources as described above and as seen in Figs. 2 and 3. The distribution in  $B - V$  has a bimodal distribution with the red peak attributable to disk stars and the blue to halo stars. Predictions from the Bahcall & Soneira models are plotted alongside the observations and shown in terms of the disk and spheroid components. Again, many features in the observed distributions are matched by the models, but with less success for the mid-Galactic latitudes shown in Fig. 6. We did not attempt to fit the data with the model, of course, and it is possible that the model parameters could be adjusted to match the observations more closely. For the mid-Galactic latitudes, an overabundance of objects relative to the model predictions for  $0.4 < B - V < 1.2$  suggests that more halo stars are present than predicted by the model. The distribution in  $B - V$  appears to be a better discriminator between the two components than the distribution in  $V$  shown in Fig. 2.

While most objects lie between  $B - V = 0.4$  and 1.8, there are tails in the distribution showing that a few objects have extreme colours. The model does not predict as many of the bluest objects as are observed. The bluest objects will presumably include white dwarfs, CVs, and emission-line objects, and are a prime target for our follow-up classification spectroscopy. Results of the spectra will be discussed in future publications.

**Figure 2.** The number of point sources observed vs.  $V$  towards a mid-galactic latitude area at  $b = +23^\circ$   $l = 200^\circ$  (fields 13-18) is shown by the solid line in panel (a). Here we require stellarity $>0.8$  to include only point sources. The dashed line in panel (a) shows the predicted  $V$ -distribution for the fields according to the Galaxy model of Bahcall & Soneira. Panel (b) shows the total number of stars predicted by the Bahcall & Soneira model (solid line), and the contributions to the total from the disk (dashed line) and spheroid (dot-dashed line) components.

**Figure 3.** The number of point sources observed vs.  $V$  towards the North Galactic Pole (fields 19-24) is shown by the solid line in panel (a). A comparison with the Galaxy models of Bahcall & Soneira is made. See caption to Fig. 2 for details.

## 4.2 Photometric Variability

The most unique aspect of the FSVS dataset is the variability information available for each source. The  $V$ -band light curves show that photometric variability is detected in a few percent of the sources. These variations take place on all of the timescales sampled, from  $\sim 13$  minutes to about five days. The amplitudes of variation also display a wide range, from about 5 millimagnitudes (or the minimum amplitudes we could detect) to about one magnitude.

Our sensitivity to detecting photometric variations is a function of the source brightness because sources detected with higher numbers of counts can be measured (photometrically) to a higher precision. To demonstrate our photometric precision as a function of magnitude, we plot the logarithm of the standard deviation measured in the data points in each light curve versus the mean  $V$ -magnitude in Fig. 8. Here we include only point sources by requiring a stellarity $>0.8$ . Since most sources do not vary, the standard deviations of their light curves reflect the uncertainty in measuring each data point based on counting statistics and these data trace out the locus of a precision vs. magnitude function. The data points in Fig. 8 are shown as either dots or X's. Light curves whose reduced  $\chi^2$  statistic ( $\chi_\nu^2$ ) for a constant fit to the light curve is greater than 10 are represented by the X's. These stars are variable at a very high level of confidence. The dots represent stars with smaller values of  $\chi_\nu^2$ . Obviously on this plot variable sources tend to lie above the non-variable sources. There is no distinct dividing line between the two, however, because variable observing conditions mean some fields are observed to higher precision than others as well as the fact that the calculation of  $\chi_\nu^2$  is a weighted one while that of  $\sigma$  is unweighted. The threshold of  $\chi_\nu^2 = 10$  is arbitrary, but adopting a high value prevents the misidentification of non-variable objects as variable since sporadic events (e.g., cosmic rays or asteroids in the aperture) can interfere with our photometry.

To select a sample of variable objects from our data tables, we apply statistical tests to each light curve. Our first approach is to calculate the  $\chi_\nu^2$  statistic for a constant fit to each light curve and to determine the likelihood that

**Figure 4.** A plot of  $B - V$  vs.  $V - I$  for point sources (stellarity $>0.8$ ) found in the FSVS. Most stars lie along the main sequence while a few outliers may be seen. The  $V - I$  colors of main sequence stars are labelled along the top of the plot for reference.

**Figure 5.** A plot of  $B - V$  vs.  $V - I$  for extended sources (stellarity < 0.2) found in the FSVS. Many of these galaxies cluster below the stellar main sequence on this plot (see also Fig. 4) while others are coincident with the colours of main sequence or giant stars.

**Figure 6.** Panel (a) shows the number of point sources observed vs.  $B - V$  towards a mid-galactic latitude area at  $b = +23^\circ$   $l = 200^\circ$  (fields 13-18) as a solid line. Here we require stellarity > 0.8 to include only point sources. The dotted line shows the predicted  $B - V$  distribution for these fields according to the Galaxy model of Bahcall & Soneira. Panel (b) shows the same model prediction as a solid line as well as the spheroid and disk components as dot-dashed and dotted lines respectively.

the observed variations are not due to random fluctuations alone. Sources that are found to be variable at a high level of confidence are visually inspected on the images for any unforeseen problems and their light curves are assigned into “bins” by visual inspection and automated testing for different types of variability. We have targeted many of these variable objects with follow-up classification spectroscopy and more detailed photometry to determine their nature.

We show light curves for several variable point sources in Fig. 9. Individual observations are spaced from approximately 13 minutes apart (two consecutive 10-minute exposures with a 3-minute readout time) up to 5 days. Photometric variations are seen with both short- and long-term behaviour, enabling us to create descriptive classifications for each variable object (slow variations, rapid variations, low- or high-amplitude variations, periodicity, etc.)

Periodic variations are actually difficult to detect given the limited number of datapoints in the FSVS light curves. However, visual inspection of the light curves does show a few suggesting periodic variations. Several types of periodic and semi-periodic variable stars are likely to show up in our dataset. These include chromospherically active late-type dwarfs, which show modulations in time with their rotational period as spots move into and out of the observer’s direction, eclipsing binaries of many types, pulsating variables, and interacting binaries.

RR Lyrae stars are likely to be present in the FSVS and good candidates are drawn from those stars having variability on hour time scales and with colours consistent with this class (panel (b) in Fig. 9 shows the light curve of a candidate RR Lyr star). Follow-up time-series photometry can confirm their type and, from their magnitudes, their distances can be estimated.

Since the FSVS is very rich in late-type dwarfs, it is therefore also likely to contain a large number of spotted variables. Indeed we see many stars having slow variations over a 5-day time interval with amplitudes ranging from several tenths of a magnitude down to the smallest amplitudes we can detect. Panels (a) and (d) in Fig. 9 show light curves with this type of behaviour. An analysis of variability versus colour (and by implication, spectral type) will show how often this affects the different late-type dwarf populations.

**Figure 7.** Same as for Fig. 6, but for fields 19-24 at the North Galactic Pole.

**Figure 8.** The logarithm of the observed standard deviation in the light curves of FSVS point sources (stellarity > 0.8) vs. their mean  $V$ -magnitudes for all 30 fields listed in Table 1. Only light curves with 8 or more error-free detections are included. Light curves with  $\chi^2_\nu > 10$  are high probability variables and are shown as X’s. The standard deviations found for the remaining sources are shown as dots.

**Figure 9.** Light curves of variable point sources. For panels (a) through (d), the spacing between consecutive data points is  $\sim 43$  minutes on the first night and 13 minutes on the last night. The CV star in panel (e) (GO Com) is observed in the same manner as the others on the first night and with exposures 13 minutes apart on the second night. For panels (a) through (d) the zeropoint in time is set to HJD=2451134 and for panel (e) the zeropoint in time is set to HJD=2451313. Error bars in magnitude are shown in panels (a) and (d). In panels (b), (c), and (e), the errorbars are the same size or smaller than the points.

Without the variability information in the FSVS, rare classes of objects having colours comparable to those of “normal” stars or other objects may go unidentified. For example, one of the main goals of the FSVS is to search for the existence of faint, low mass-transfer rate cataclysmic variable stars (CVs are interacting red dwarf-white dwarf pairs; see Warner 1995). CV candidates would be selected on the basis of rapid variability. The cataclysmic variable GO Comae was observed in field 23 and its light curve is shown in panel (e) of Fig. 9. The colours are relatively blue ( $B - V = -0.2$  and  $V - I = 0.9$ ), but this object is most effectively identified via its rapid and high-amplitude variations. Much of the variation in this object is attributable to flickering, although a possible 95-minute period may produce some variations as well (Howell et al. 1990). Candidate CVs will be targeted for follow-up spectroscopy and confirmation would be made by detecting the characteristic broad emission lines in their spectra.

### 4.3 Trans-Neptunian Objects

We searched three ecliptic opposition fields taken during the November 1998 run for trans-Neptunian objects (TNOs, also known as Kuiper Belt objects), using a moving-object detection code written by one of us (HS). To detect TNOs, fields near opposition are needed in order to distinguish TNOs from main-belt asteroids and other objects based on their motion. We found no TNO candidates in these fields.

We expected to find one known TNO, 1997 CS29, within the search area. The predicted position for this TNO fell within one of our observed ecliptic opposition fields on 1998 Nov 16 UT. However, 1997 CS29 was not found, probably due to a bright saturated star located at its expected position.

Although the limiting magnitudes of many of the images from the November run were as faint as  $V = 25$ , for detection of moving objects, three, or preferably four images at different times need to be intercompared. The variable observing conditions during the November run resulted in the sets of three or four exposures having varying limiting magnitudes, and our detection sensitivity is limited by the quality of the

poorest image in the set. As a result, the effective limiting magnitude for our search was  $V = 23.5 - 24$ .

Given this limiting magnitude, over the 0.81 square degrees searched, we would have expected to find 0.5 - 1 TNOs on average, based on the TNO luminosity function determined by Gladman et al. (1998). We used the mean  $V - R$  of known TNOs to apply the  $R$  luminosity function of Gladman et al. to our  $V$  observations. This is consistent with our negative result. In better weather conditions we can expect consistent limiting magnitudes of  $V > 25.5$  (similar to the best of our November 1998 frames), and the expected number of TNOs then rises to several per field. Thus we will continue to search future FSVS opposition fields for TNOs.

## 5 CONCLUSIONS

The Faint Sky Variability Survey is an ongoing deep, wide-field, multi-colour, time-series CCD survey towards moderate and high galactic latitudes. Hundreds of thousands of objects in the magnitude range  $V = 17 - 25$  are observed for classification on the basis of  $BVI$  colours, temporal and astrometric variability, and morphology. Analysis of the FSVS light curves reveals variable objects of many types, objects with unusual colours, and will soon be extended to include high proper motion stars. Interesting populations have been observed spectroscopically and will be discussed in future publications.

## ACKNOWLEDGMENTS

PJG and PMV are partially supported by NWO Spinoza grant 08-0 to Ed van den Heuvel. PJG is currently a CfA fellow. SBH acknowledges partial support of this project by NSF grant AST9818770. MEH is partially supported by the Wyoming Space Grant Consortium NASA grant #NGT-40008. The FSVS is based on observations made through the Isaac Newton Groups' Wide Field Survey Programme with the Isaac Newton Telescope operated on the island of La Palma by the Isaac Newton Group in the Spanish Observatorio del Roque de los Muchachos of the Instituto de Astrofísica de Canarias.

## REFERENCES

- Bahcall J.N., Soneira R.M., 1980, *ApJS*, 44, 73  
 Bertin E., Arnouts S., 1996, *A&AS*, 117, 393  
 Cox A., 2000, editor, *Allen's Astrophysical Quantities* 4th edition, Springer-Verlag, New York  
 Everett M.E., Howell S.B., in preparation  
 Gladman B., Kavelaars J.J., Nicholson P.D., Loredó T.J., Burns J.A., 1998, *AJ*, 116, 2042  
 Groot P. et al., 2000, *MNRAS*, (paper I)  
 Hartwick F.D.A., Schade D., 1990, *ARA&A*, 28, 437  
 Honeycutt R.K., 1992, *PASP*, 104, 435  
 Howell S.B., Mitchell K.J., Warnock III A., 1988, *AJ*, 95, 247  
 Howell S.B., Szkody P., Kreidl T.J., Mason K.O., Puchnarewicz E.M. 1990, *PASP*, 102, 758  
 Leggett S.K., 1992, *ApJS*, 82, 351  
 Monet D. et. al., 1996, USNO-SA1.0. U.S. Naval Observatory, Washington DC

Warner B., 1995, *Cataclysmic Variable Stars*. Cambridge Univ. Press, Cambridge

This paper has been produced using the Royal Astronomical Society/Blackwell Science L<sup>A</sup>T<sub>E</sub>X style file.

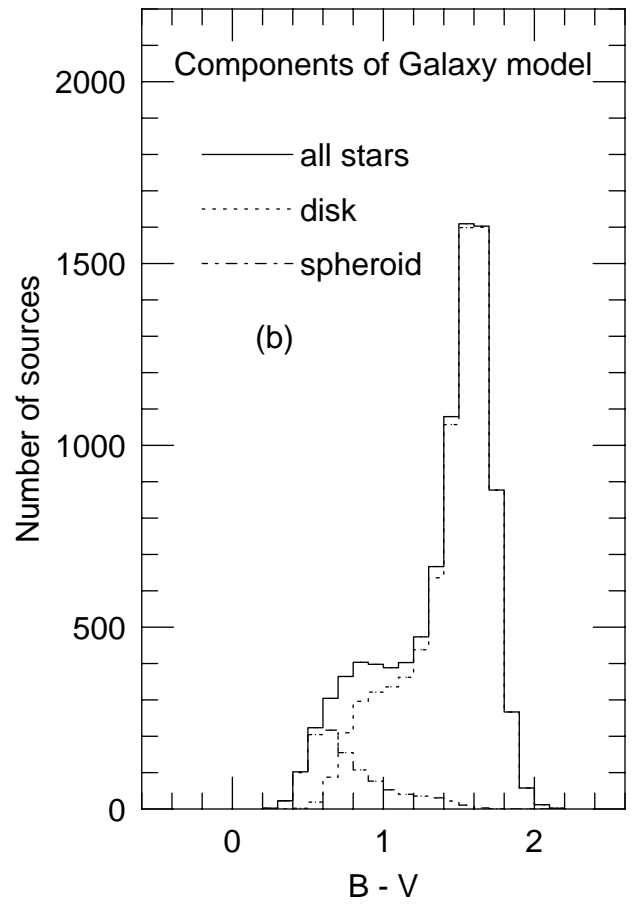
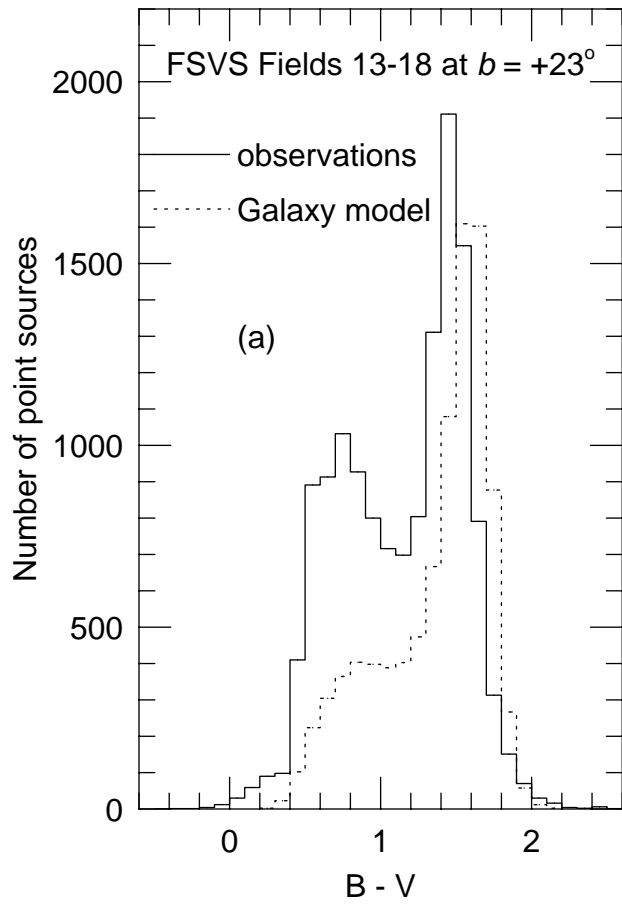
This figure "BVIplot\_gal.jpg" is available in "jpg" format from:

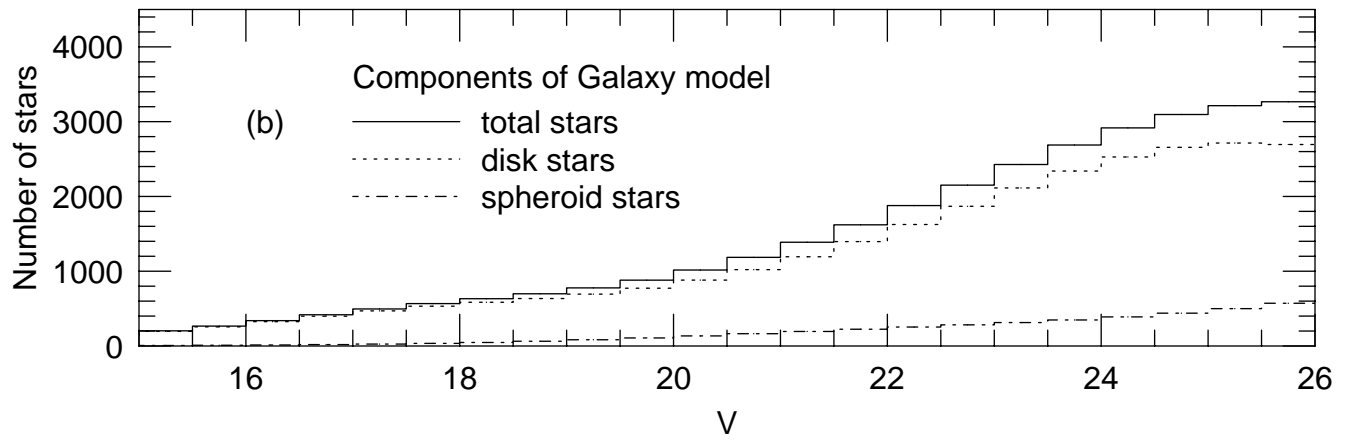
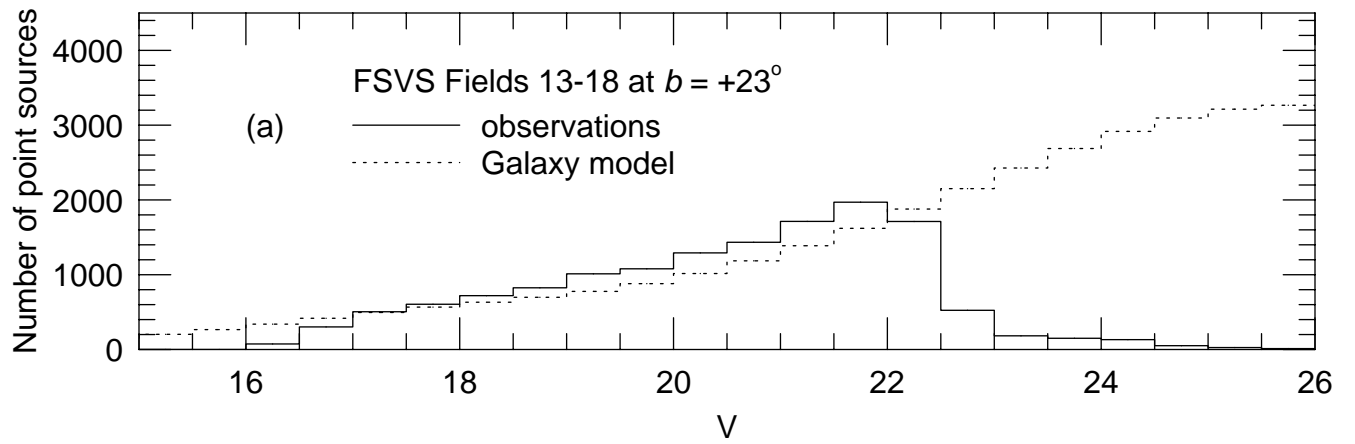
<http://arxiv.org/ps/astro-ph/0009479v1>

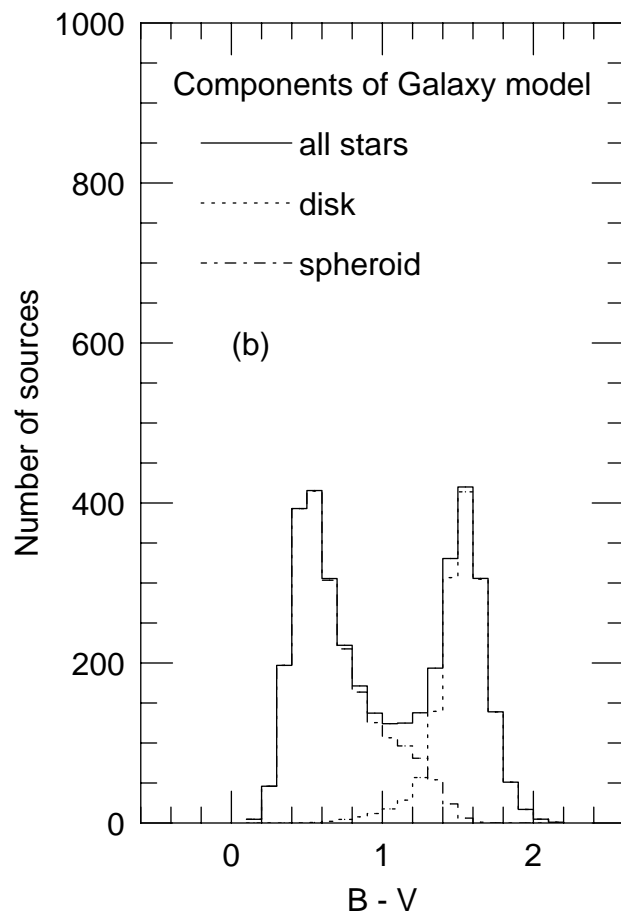
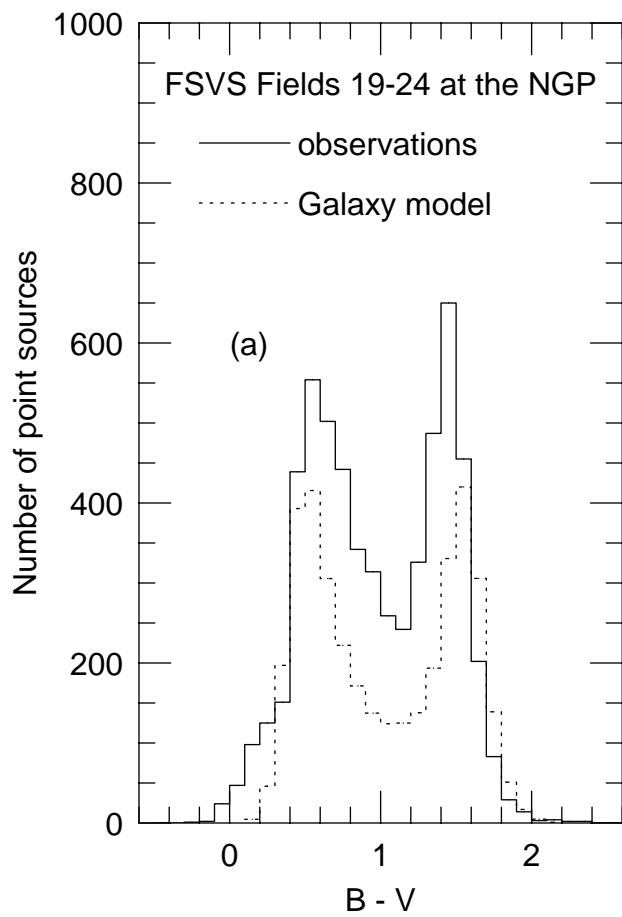
This figure "BVIplot\_star.jpg" is available in "jpg" format from:

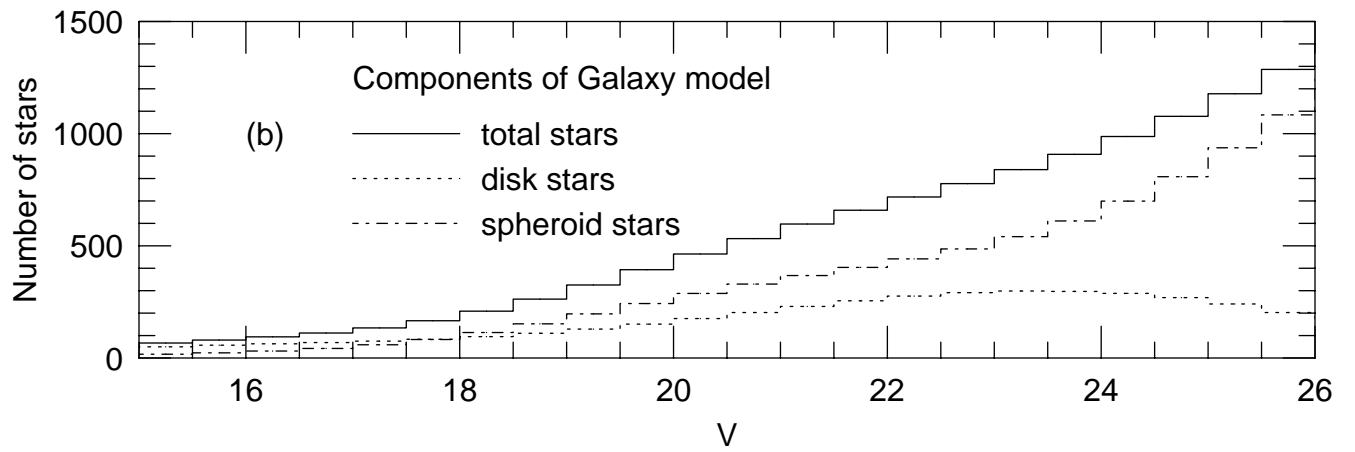
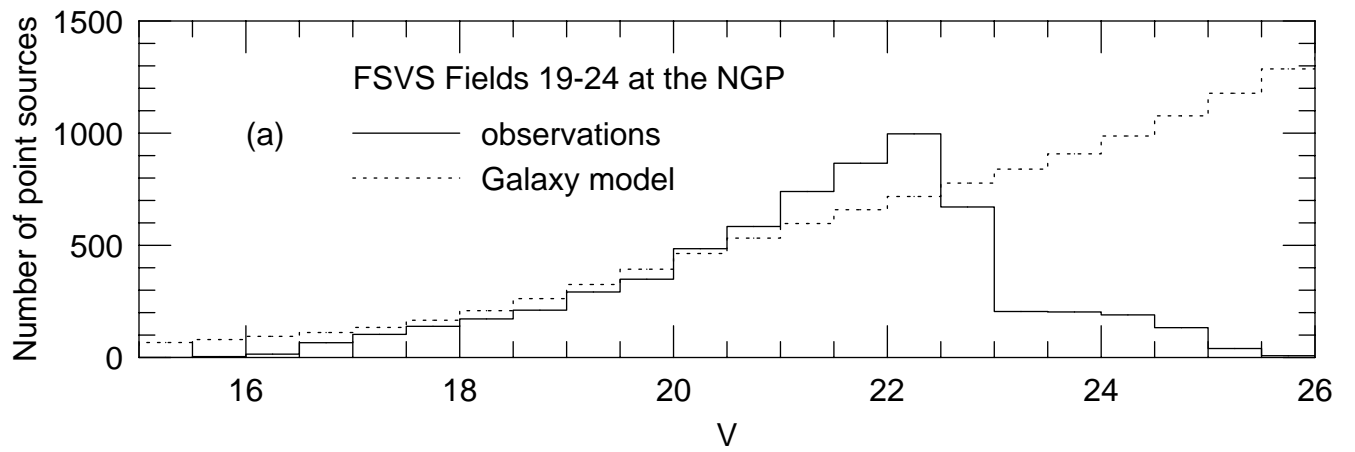
<http://arxiv.org/ps/astro-ph/0009479v1>

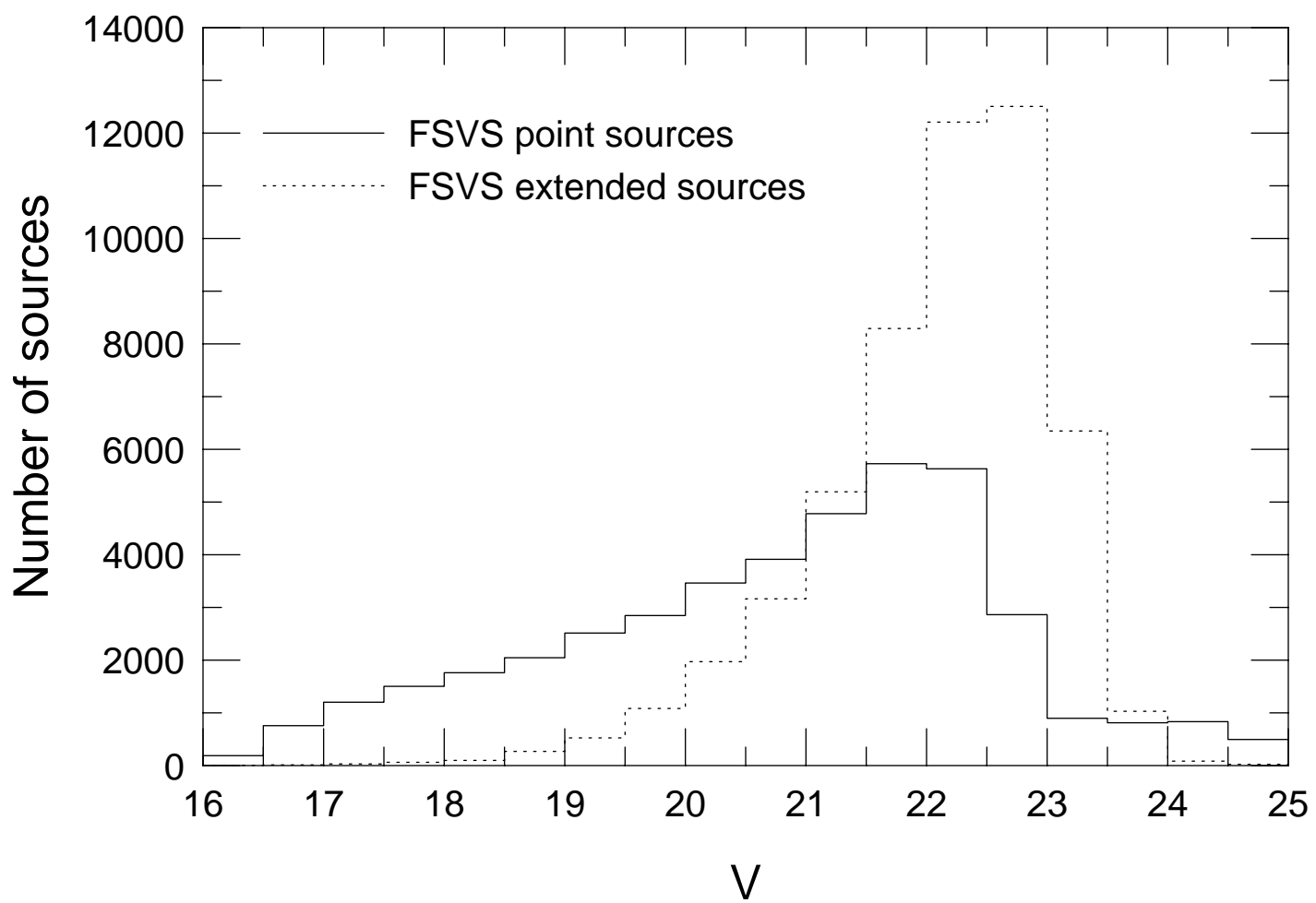












This figure "stddev\_mag.png" is available in "png" format from:

<http://arxiv.org/ps/astro-ph/0009479v1>

